Macromolecules
ARTICLE

Macromolecules **2010**, *43*, 461–466 **461**
DOI: 10.1021/ma901987q

Orientation of Block Copolymer Resists on Interlayer Dielectrics with Tunable Surface Energy

Hyo Seon Suh,[†,‡] Huiman Kang,[§] Chi-Chun Liu,[§] Paul F. Nealey,[§] and Kookheon Char*[,†,‡]

[†]*Interdisciplinary Program in Nano-Science and Technology,* [‡]*Center for Functional Polymer Thin Films and School of Chemical and Biological Engineering, Seoul National University, Seoul 151-744, Korea, and* [§]*Department of Chemical and Biological Engineering, University of Wisconsin-Madison, Madison, Wisconsin 53706*

Received September 5, 2009; Revised Manuscript Received October 30, 2009

ABSTRACT: It has been well established that one of most important factors to control the orientation of microdomains in block copolymer (BCP) films is the wetting behavior of a BCP at the interface (or on a substrate). From this perspective, we studied the wetting behavior of P(S-*b*-MMA) thin films on organosilicate (OS) interlayer dielectric layers (ILDs), which were employed as the target substrates for patterning by BCP lithography. We controlled the surface energy of OS substrates by varying the cure temperature of OS substrates ranging from 200 to 400 °C. As the cure temperature was increased, the wetting behavior of a P(S-*b*-MMA) film on the OS substrate changed from the asymmetric to the symmetric wetting, as confirmed by AFM, which, in turn, allowed us to find the optimal cure temperature for neutral wetting behavior. As a result, we obtained perpendicularly oriented BCP microdomains on the OS substrate cured at 360 °C without further surface modification. Finally, we were able to transfer sub-25 nm BCP patterns directly onto the neutral ILD layers through reactive ion etching. The process approach taken here clearly demonstrates that the process involved in BCP lithography could be simplified by eliminating the additional surface modification step on a target substrate.

Introduction

Recently, block copolymer (BCP) thin films have gained great attention as emerging resist materials for next generation lithographic technology.[1] They can self-assemble to well-defined periodic patterns with sub-25 nm size, for which it is difficult to obtain through the conventional photolithographic techniques.[2−6] For the lithographic applications of BCP thin films, we need BCP films with phase-separated microdomains perpendicularly oriented to the bottom substrate to be used as nanotemplates for the pattern transfer by the reactive ion etching (RIE) process. However, in most of the cases with BCP films, preferential interaction of either of the blocks with the interfaces (i.e., bottom substrate and free surface) cause the parallel orientation of such microdomains.[7−9] To overcome this limitation in the perpendicular orientation of microphase-separated domains, several works have been done on the surface modification to balance the interfacial interactions of blocks with interfaces.[10−21] The most well-noted approach is to modify the substrate by grafting random copolymer brushes on the bottom substrate.[10] By controlling the composition of random copolymer brushes, the interfacial interactions of blocks with the modified substrate can be balanced. As a result, microdomains can perpendicularly orient to the bottom substrate because of the neutral wetting behavior of BCP films. Recently, more rapid and generic methods to generate a energetically neutral surface have been reported, overcoming the drawbacks of the previous approach such as the slow process to anchor brushes to the substrates and the limitation that the bottom substrate should be oxide surfaces.[17−19] In these cases, thermal or UV cross-linkable units were introduced to the backbones of random copolymer chains. These moieties make the neutral brushes insoluble to the BCP solutions by thermal or UV treatment. Although cross-linkable brush systems successfully reduce the process time and, at the same time, remove the limitation of bottom substrates, they still require additional surface treatment on the substrates to form nanoscale patterns with BCP resist films.

Here we introduce a new concept to generate energetically neutral interlayer dielectrics (ILDs), which can orient the microphase-separated BCP domains (patterns) perpendicular to the ILD surface. The main advantage of this approach is to eliminate the additional surface modification step on substrates (typically, ILDs for semiconductor industry) by grafting neutral brushes. Our ILD insulator used in this study is the spin-on organosilicate (OS) glass, and its prominent dielectric and mechanical properties can be controlled by thermal treatment on spin-coated films, called the cure process.[22,23] Instead of controlling the chemical composition of the surface-modifying layer to balance the interfacial interactions with the substrate, we controlled the cure temperature of the OS substrates. We found the optimal cure temperature for the OS films to realize energetically neutral substrates for P(S-*b*-MMA), causing the perpendicular orientation of P(S-*b*-MMA) films on the OS substrates. The structure and orientation of microdomains within the P(S-*b*-MMA) resist films were investigated with AFM and GISAXS analyses. Finally, we were able to transfer sub-25 nm BCP patterns directly onto the ILD insulators through RIE.

Experimental Section

Materials. OS used as the bottom substrate was synthesized by the sol−gel reaction with methyltrimethoxysilane (MTMS, Aldrich) and 1,2-bis(trimethoxysilyl)ethane (BTMSE, Aldrich). The detail synthetic procedure is described elsewhere.[22] The feed ratio of MTMS and BTMSE was 9/2 by mol %. Polystyrene-*block*-poly(methyl methacrylate) (PS-*b*-PMMA) diblock copolymer was

*Corresponding author. E-mail: khchar@plaza.snu.ac.kr. Tel: +82-2-880-7431. Fax: +82-2-873-1548.

Published on Web 11/13/2009

purchased from Polymer Source. The molecular weight of diblock copolymer was 104 kg/mol (52K−52K) with a polydispersity index of 1.09. The domain spacing (L_0) measured by small-angle X-ray scattering (SAXS) experiments was 47 nm.

Film Preparation. The 100 nm thick OS films were prepared by spin coating with 5 wt % of OS solutions dissolved in methyl isobutyl ketone (MIBK) on clean Si wafers. The OS films were cured at the desired temperature for 6 h with a homemade furnace under N_2 purge. On the thermally cured OS substrates, P(S-*b*-MMA) films were spin-cast from 2 and 3 wt % solution of P(S-*b*-MMA) in toluene resulting in ~85 nm (~$1.8L_0$) and ~105 nm (~$2.2L_0$) thick BCP films, respectively. The BCP films placed on OS substrates were annealed at 190 °C for 3 days in vacuum.

Pattern Transfer Using BCP Resists. Pattern transfer to OS substrates using BCP resists was accomplished by a Plasma-Therm/Unaxis 790 reactive ion etcher (RIE). O_2 RIE (for 80 s at 10 mTorr and 50 W with O_2 flow rate of 10 sccm) was performed to remove selectively PMMA domains from the BCP film. CF_4 RIE (for 60 s at 10 mTorr and 100 W with CF_4 flow rate of 50 sccm) following the O_2 RIE was performed to etch into the OS substrate using the residual PS patterns as an etching mask. The remaining PS resists were further removed by the oxygen plasma etching process as the final step.

Characterizations. FT-IR measurements were performed on a JASCO FT/IR 200 spectrometer; 64 accumulations were signal-averaged at a resolution of 4 cm^{-1}. Baseline-corrected infrared spectra were obtained for thermally cured OS films on silicon wafers in absorption mode at room temperature. Static contact angles of water and diiodomethane on thermally cured OS films were measured using a DSA 100 drop shape analysis system (Kruss GmbH). The surface morphologies of BCP thin films were obtained with an atomic force microscope (AFM, Digital Instrument, Nanoscope IIIA) in tapping mode. The 45° tilted cross sections of BCP/OS films were imaged by a field emission-scanning electron microscope (FE-SEM, LEO 1550-VP). GISAXS measurements were carried out at the 4C2 beamline of the Pohang light source. The sample-to-detector distance was 2.22 m, and the wavelength of X-ray was 1.38 Å. A 2D position-sensitive detector with 1042 pixels × 1042 pixels was used to collect data. The incident angle was fixed at 0.15°.

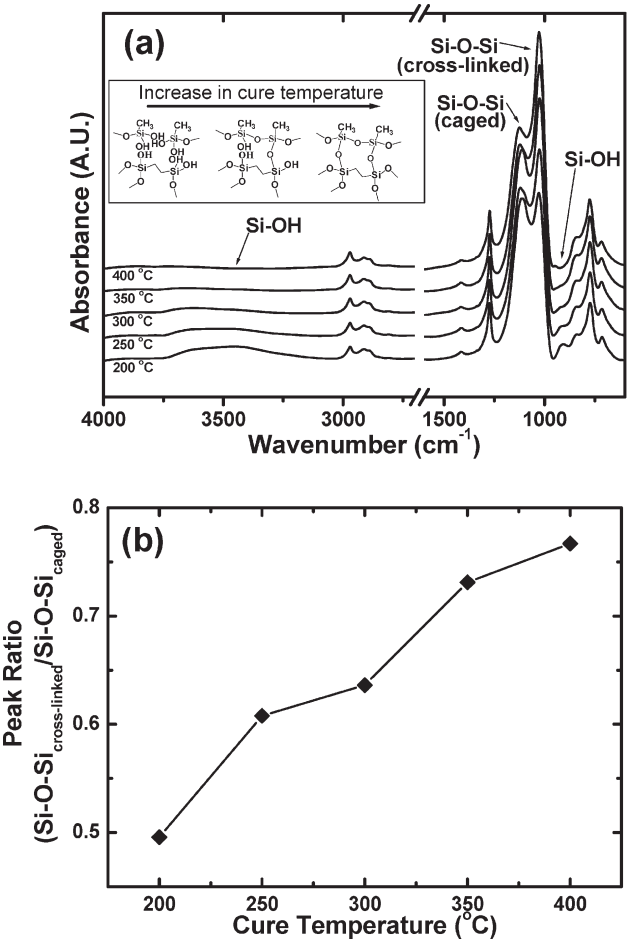

Figure 1. (a) FT-IR spectra of OS films cured at different temperature. Inset represents the structural change in OS films with the increase in cure temperature. (b) Peak ratio between cross-linked and caged Si−O−Si bonds plotted against cure temperature.

Results and Discussion

The insulating material used in this study was methylsilsesquioxane-based OS prepared by acid-catalyzed hydrolytic condensation.[22] By controlling the synthetic condition, we could generate soluble spin-on OS materials. The OS films prepared by the spin coating have initially a considerable amount of silanol (Si−OH) groups formed during the hydrolytic condensation reaction. As illustrated in the inset of Figure 1a, the thermal treatment (i.e., cure) converted these silanol groups into Si−O−Si bonds by the condensation reaction among the silanol groups.

Changes in FT-IR spectra shown in Figure 1a reveal such changes in the chemical structure of OS.[24] When we increase the cure temperature of an OS film from 200 to 400 °C, the O−H stretching band at ~3400 cm^{-1} and Si−OH stretching band at ~930 cm^{-1} decrease. These changes in the bands related to Si−OH indicate the decrease in the amount of silanol groups in OS films as the cure temperature is increased. We have also found that the condensation reaction lowering the amount of silanol groups strongly depends on the cure temperature and time. In the present study, however, the cure time is fixed at 6 h, which is sufficient to reach the steady-state degree of condensation at a specified temperature. This experimental protocol would allow us to control the amount of silanol groups by simply varying the cure temperature, which eventually affects the surface energy of the OS films.

We could also observe the changes in doublet Si−O−Si stretching bands at ~1030 and 1130 cm^{-1}. It is noted that the band at the higher frequency, assigned to short Si−O−Si chains, decreases, whereas the band at lower frequency, due to the extended Si−O−Si chains, became more intensified with the increase in cure temperature. As shown in Figure 1b, the peak ratio between the lower and the higher frequency Si−O−Si bands increases as the cure temperature is increased. The increase in this ratio reflects the conversion of Si−O−Si chains from locally cross-linked structures, such as fully or partially caged silsesquioxanes, to extended ladder-like silsesquioxanes. This type of spectral change also leads to the evidence of thermal cross-linking in the OS film. When spun-cast OS films were cured at temperature higher than 200 °C, those films were insoluble in toluene, which is the good solvent of P(S-*b*-MMA). Consequently, we could safely place P(S-*b*-MMA) BCP resist films on thermally cured OS substrates by spin coating.

Controlling the amount of hydrophilic silanol groups with thermal treatment makes it possible to control the surface energy of OS films. To estimate the surface energies of thermally cured OS films, interfacial tension measurements were carried out with the two-liquid harmonic method.[25] This method is better suited for the surfaces with low surface energy, such as polymers and OS we employed for the present study. We used water and diiodomethane as contact test liquids, and their surface tension parameters were taken from the literature.[26] The static contact angles of water and diiodomethane at room temperature on OS films cured at temperature ranging from 200 to 400 °C are shown in Table 1. As the thermal treatment temperature of OS films is increased, the contact angles measured with both contacting

Table 1. Contact Angles of Water and Diiodomethane (CH_2I_2) on OS Substrates Cured at Different Temperature

cure temperature (°C)	θ_{water} (°)	$\theta_{diiodomethane}$ (°)
200	77.24 ± 0.71	50.80 ± 0.36
250	81.28 ± 0.43	51.66 ± 0.18
300	85.54 ± 0.33	52.36 ± 0.31
350	90.04 ± 0.61	55.46 ± 0.23
400	94.42 ± 0.67	57.54 ± 0.33

liquids increase. Qualitatively speaking, the increase in contact angle indicates that the OS films become more hydrophobic as the curing temperature is increased, which is consistent with the decrease in amount of hydrophilic silanol group in the OS films. The surface energies calculated with the contact angle data in Table 1 are shown in Figure 2a. The surface energies, which are known to be the sum of dispersive and polar fractions, of the OS films decrease from 42.84 ± 0.31 to 33.64 ± 0.32 mJ/m^2 as the OS cure temperature is increased from 200 to 400 °C. This decrease in the total surface energy is dominated by the changes in the polar contribution compared with the contribution from the dispersive ones, because the amount of Si−OH (silanol) groups, the origin of polar fractions, is easily varied by the condensation reaction through thermal treatment, whereas the amount of thermally stable Si−CH_3 groups, the origin of dispersive fractions, does not significantly change.

We found that the surface energies of both PS (40.7 mJ m^{-2}) and PMMA (41.1 mJ m^{-2}) are placed within the range of surface energy that OS in this study can have.[27] Consequently, we could balance the interfacial interactions of each block in the BCP (PS-*b*-PMMA) with the OS substrate by tuning the surface energy of the OS substrate by adjusting the cure temperature. To predict accurately the balance of interactions, we need to use the values of surface and interfacial energies at the annealing temperature of P(S-*b*-MMA) (190 °C in present study). However, it was not feasible to measure all surface and interfacial energies at the anneal temperature. Instead, we have used the values at room temperature and extended to the anneal temperature based on the surface excess entropy value describing the temperature dependence of surface tension to predict qualitatively the wetting behavior of a P(S-*b*-MMA) film on the OS substrate, as Peters and coworkers studied for the substrate modified by self-assembled monolayers.[16]

To estimate the interfacial energy of either PS or PMMA block against the OS substrate, we used the harmonic mean equation shown in eq 1[28]

$$\gamma_{\text{polymer-OS}} = \gamma_{\text{polymer}} + \gamma_{\text{OS}} - \frac{4\gamma_{\text{polymer}}{}^{\text{d}}\gamma_{\text{OS}}{}^{\text{d}}}{\gamma_{\text{polymer}}{}^{\text{d}} + \gamma_{\text{OS}}{}^{\text{d}}} - \frac{4\gamma_{\text{polymer}}{}^{\text{p}}\gamma_{\text{OS}}{}^{\text{p}}}{\gamma_{\text{polymer}}{}^{\text{p}} + \gamma_{\text{OS}}{}^{\text{p}}} \quad (1)$$

where $\gamma_{\text{polymer-OS}}$ is the interfacial energy between polymer and OS, γ is the total surface energy, γ^{d} is the dispersive component, and γ^{p} is the polar component of the surface energy. The subscript "polymer" refers to the surface energy parameter of either PS or PMMA block taken from ref 27, and the subscript "OS" refers to the surface energy parameters of OS obtained from the two-liquid harmonic method mentioned earlier.

Figure 2b shows the estimated interfacial energies of PS and PMMA blocks against the OS substrate as a function of cure temperature of OS. It is found that the interfacial energy of PMMA block against OS ($\gamma_{\text{PMMA-OS}}$) has its minimum when the OS film is cured at 250 °C, which is the cure temperature that makes the surface energy of OS closest to that of PMMA block. When the OS film is cured at temperature above 250 °C, the surface energy difference between PMMA and OS becomes larger and, consequently, $\gamma_{\text{PMMA-OS}}$ is increased. The interfacial energy

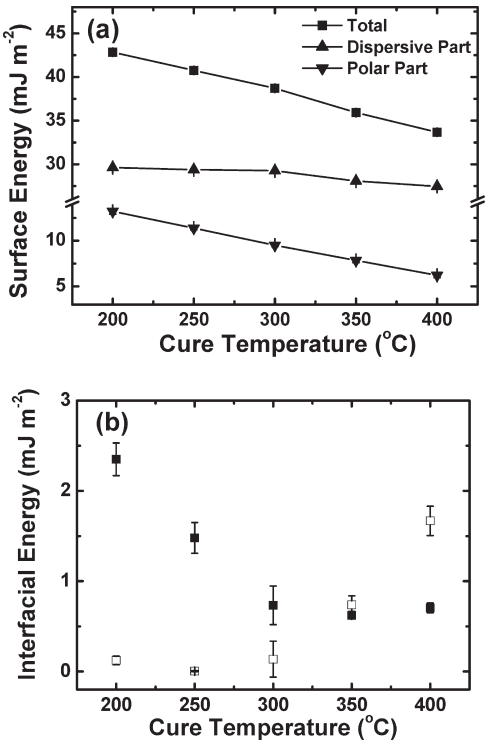

Figure 2. (a) Surface energy of OS substrate as a function of cure temperature. Total surface energy (■) is the sum of dispersive (▲) and polar part (▼). (b) Interfacial energies of PS (■) and PMMA (□) blocks against the OS substrate plotted against cure temperature.

between PS block against the OS surface ($\gamma_{\text{PS-OS}}$) has its minimum when the OS film is cured at 350 °C, and the interfacial energy slightly increases at curing temperature above 400 °C. It is noteworthy that these two interfacial energies, $\gamma_{\text{PMMA-OS}}$ and $\gamma_{\text{PS-OS}}$, are almost identical when the OS film is cured at ~350 °C.

We placed P(S-*b*-MMA) films by spin-coating on thermally precured OS substrates and annealed the BCP films at 190 °C, which is lower than the precure temperature for the OS substrates. During the thermal annealing of the BCP films, we noted that the surface energy of the OS substrate did not change significantly. Because the degree of hydrolytic condensation between silanol groups to form siloxane in the OS substrates depends on the highest temperature of thermal treatment (during combined cure process of the OS substrates and the annealing process of BCP films), we expect that the wetting behavior of a P(S-*b*-MMA) film on the OS substrate during the BCP annealing step is based on the interfacial energies of each block against the OS substrate, as estimated from Figure 2b. The OS substrate cured at temperature below 250 °C has preferential interaction with the PMMA block because $\gamma_{\text{PMMA-OS}}$ is much lower than $\gamma_{\text{PS-OS}}$ according to our estimation. (See Figure 2b.) Under this condition, the PMMA blocks are preferentially wet on the bottom OS interface, whereas the PS blocks cover the free surface (because of lower surface energy), leading to a microdomain orientation parallel to the OS substrate. When the thickness of P(S-*b*-MMA) film is off commensurable condition ($(n + 1/2)L_0$, where n is the integer number and L_0 is the domain spacing of lamellae), hole or island structure with the height of L_0 at the free surface of films is observed because of the asymmetric wetting nature of the BCP film, as confirmed in Figure 3a,b,f,g.

On the other hand, there is no energetically preferential wetting of either block against the OS substrate when the substrate is cured at 360 °C because the two values between $\gamma_{\text{PMMA-OS}}$ and $\gamma_{\text{PS-OS}}$ become almost identical. (See Figure 2b.) This is to say

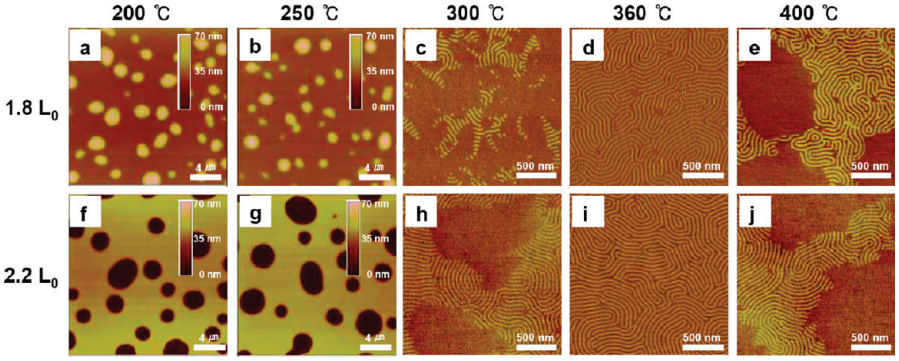

Figure 3. (a,b,f,g) AFM height and (c,d,e,h,i,j) phase images of P(S-*b*-MMA) films annealed at 190 °C for 3 days in vacuum placed on OS substrates precured at different temperature. The film thickness of P(S-*b*-MMA) is ~1.8L_0 for parts a−e and the film thickness for parts f−j is ~2.2L_0.

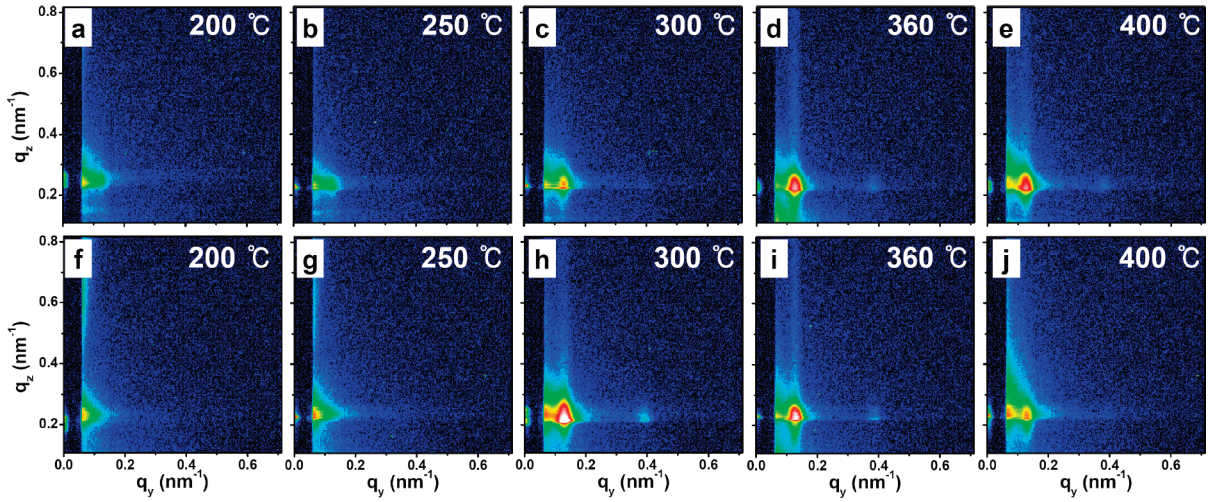

Figure 4. GISAXS patterns obtained from P(S-*b*-MMA) films placed on OS substrates cured at different temperature. The film thickness of P(S-*b*-MMA) is ~1.8L_0 for parts a−e and the film thickness for parts f−j is ~2.2L_0. The X-ray incidence angle is fixed at 0.15°.

that both PS and PMMA blocks can wet the bottom OS substrate without any preference, implying the perpendicular orientation of microdomains on the OS substrate. Indeed, we observe the typical fingerprint patterns at the top surface of a P(S-*b*-MMA) film (Figure 3d,i), which have frequently been shown on the BCP films with microdomains oriented perpendicularly, when the OS substrate is cured at 360 °C.

When the cure temperature of OS substrate slightly deviates from the energetically neutral temperature (~360 °C), although the values of $\gamma_{PMMA-OS}$ and γ_{PS-OS} are not identical, the difference between these two values is not that significant. Therefore, the neutral wetting behavior of P(S-*b*-MMA) competes with the asymmetric wetting against the OS substrate cured at 300 °C while competing with the symmetric wetting against the OS substrate cured at 400 °C. In these two cases, we observe the surface morphologies of BCP films with partial fractions of perpendicularly oriented microdomains. When the OS substrate is cured at temperature above 400 °C, both $\gamma_{PMMA-OS}$ and γ_{PS-OS} increase because of the decrease in the surface energy of OS substrate, as shown in Figure 2a. As a result, P(S-*b*-MMA) films dewet from the OS substrate instead of forming holes or islands at the free surface because of the symmetric wetting.

The grazing-incidence small-angle X-ray scattering (GISAXS) studies in conjunction with the corresponding AFM images of the same samples can reveal more information on the inner structure of the BCP film as well as the surface textures.[29] Figure 4 shows the GISAXS patterns from the corresponding BCP films shown in Figure 3. To obtain the information on BCP films with minimal influence of the scattering from the OS substrate, we fixed the incidence angle of X-ray beam at 0.15°, which is below the critical angle of OS (0.151°, as confirmed by X-ray reflectivity (XRR), see the Supporting Information) and above the critical angle of PS (0.145°) and PMMA (0.132°).[30] However, it was difficult to define exactly the incident angle between 0.145 and 0.151° in our current instrumental setup. Moreover, the difference in electron density between the two blocks, which determines the scattering intensity, as well as the electron density difference between BCP and the OS substrate is not large enough for strong signal. Because of these reasons, we were not able to obtain clear GISAXS patterns. However, these GISAXS patterns can still provide enough evidence to gain insight into the internal BCP structure.

In the case of GISAXS patterns obtained from the BCP films placed on the OS substrate cured at temperature below 250 °C (Figure 4a,b,f,g), no clearly resolved scattering peaks at $q_y = 2\pi/L_o$ (0.133 nm^{-1} in this study) were observed. Instead, weak scattering patterns diffusing from the beam stop are shown. These results indicate that the lamellar BCP domains are oriented parallel to the OS substrates. In the case of GISAXS patterns from the BCP films placed on the OS substrate cured at 300 °C (Figures 4c,h), peaks diffusing from the beam stop as well as the well-defined Bragg rod peak at $q_y = 2\pi/L_o$ are shown all together. These kinds of scattering patterns reveal that the BCP films contain both parallel and perpendicularly oriented lamellar domains, which is in excellent agreement with AFM data. (See Figure 3c,h.) The GISAXS patterns from the BCP films placed on the OS substrate cured at 360 °C (Figure 4d,i) show the GISAXS patterns such that the scattering peaks diffusing from

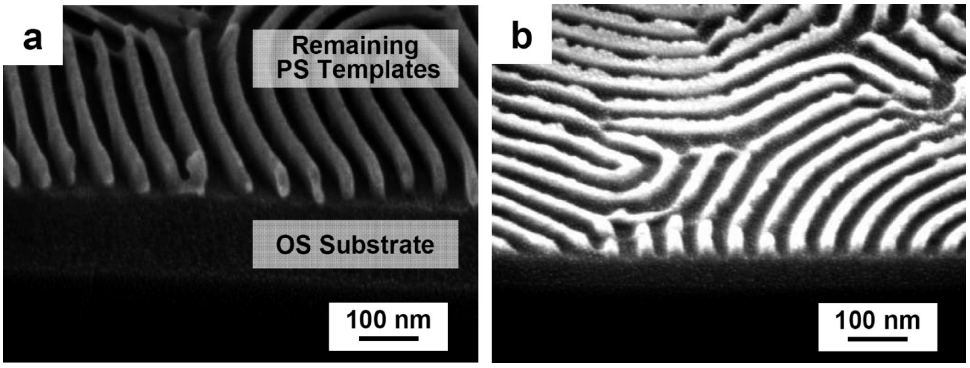

Figure 5. Pattern transfer to an OS interlayer dielectrics employing a P(S-*b*-MMA) block copolymer thin film as a nanoresist. The 45° tilted cross-sectional SEM images of (a) a PS nanoresist vertically aligned on a energetically neutral OS substrate after the selective removal of PMMA blocks using O_2 RIE and (b) a pattern-transferred OS substrate etched with CF_4 RIE using the PS block nanoresist as an etching mask.

the beam stop are much weaker, whereas the Bragg rod peak at $q_y = 2\pi/L_o$ is much more pronounced when compared with the peaks shown in Figure 4c,h. Consequently, we strongly believe that a majority of lamellar domains are oriented perpendicular to the OS substrates. The GISAXS patterns from the BCP films on top of the OS substrate cured at 400 °C (Figures 4e,j) show both diffuse and Bragg rod peaks again, indicating that the perpendicularly oriented lamellar domains coexist with the domains in parallel orientation. It is quite interesting to confirm that all GISAXS data obtained from the BCP films on OS substrates, cured at different cure temperature, are in excellent agreement with the AFM images shown in Figure 3.

In the case of P(S-*b*-MMA) resist films, the PMMA domains could be selectively removed by wet etching process to use the P(S-*b*-MMA) films as nanotemplates or resists for pattern transfer.[31] We, however, have realized in this study that the remaining lamellar PS domains easily collapse during the wet etch process because of the capillary force of solvent between lamellar domains with a high aspect ratio (larger than 4 for a 105 nm thick film). Instead of using the wet etching process, we employed the O_2 RIE process to remove PMMA domains selectively. [32] We were able to remove the PMMA domains selectively, whereas half of the thickness of the PS domains remained because the PMMA domains are etched away two times faster than the PS domains under the current RIE condition. Figure 5a shows the 45° tilted cross-sectional SEM image of a P(S-*b*-MMA) film placed on the neutral OS substrate after the selective removal of PMMA domains using RIE with oxygen gas. This SEM image also demonstrates that the perpendicular orientation in the P(S-*b*-MMA) film persists throughout the entire film thickness. Finally, we successfully transferred the patterns of a BCP resist directly to the OS substrate using RIE with CF_4 gas, an etchant for OS, as shown in Figure 5b. Within the OS layer patterned by BCP resists, it is quite possible that a small amount of silanol groups remain because the OS materials prepared in the present study could be fully cured when the OS was thermally treated at temperature above 450 °C.[24] The remaining silanol groups could slightly increase the dielectric constant and slightly decrease the elastic modulus of the OS layer when compared with fully cured OS. However, such a minor effect of lowering the cure temperature on physical properties of OS thin films could be overcome by the post treatment at temperature above 400 °C after the BCP resists are removed from the OS substrate after patterning.

Conclusions

We have demonstrated the tunability of surface energy of OS substrates to control the orientation of microdomains of BCP thin films placed on it. Without additional surface modification, we could obtain perpendicularly orientated BCP microdomains on the OS substrate by the single cure step at the optimal temperature for OS where energetically neutral conditions for both PS and PMMA blocks against OS substrates were satisfied. The novelty of the current approach lies in the fact that our OS substrate can serve not only as the energetically neutral substrate for the orientation of BCP resists but also as the insulator (interlayer dielectrics; ILDs) in massively integrated circuits, which is one of the target low-K layers to be patterned by BCP nanolithography.

Acknowledgment. This work was financially supported by the Korea Science and Engineering Foundation (KOSEF) grant funded by the Korean Ministry of Education, Science and Technology (MEST) (Acceleration Research Program (no. R17-2007-059-01000-0) and NANO Systems Institute-National Core Research Center (no. R15-2003-032-05001-0)). We also acknowledge the financial support from the MEST on graduate programs at Seoul National University through the Brain Korea 21 Program and the World Class University (WCU) Program on the Chemical Convergence on Energy and Environment (C2E2; 400-2008-0230). This work is also performed by the Collaborative Program of Nanoscale Science and Engineering Center of National Science Foundation (NSF) (DMR-0425880). We thank K. W. Kim and Y. J. Park at Pohang Light Source for assisting the GISAXS and XRR measurements.

Supporting Information Available: XRR data obtained from an OS substrate is available. On the basis of XRR data, the critical angle of the OS substrate is measured. This material is available free of charge via the Internet at http://pubs.acs.org.

References and Notes

(1) *International Technology Roadmap for Semiconductors*, ITRS 2007 Edition. www.itrs.net/Links/2007ITRS/2007_Chapters/2007_ERM.pdf.
(2) Park, M.; Harrison, C.; Chaikin, P.; Register, R.; Adamson, D. *Science* **1997**, *276*, 1401.
(3) Thurn-Albrecht, T.; Schotter, J.; Kastle, G. A.; Emley, N.; Shibauchi, T.; Krusin-Elbaum, L.; Guarini, K.; Black, C. T.; Tuominen, M. T.; Russell, T. P. *Science* **2000**, *290*, 2126.
(4) Park, C.; Yoon, J.; Thomas, E. L. *Polymer* **2003**, *44*, 7779.
(5) Segalman, R. A.; Yokoyama, H.; Kramer, E. J. *Adv. Mater.* **2001**, *13*, 1152.
(6) Fasolka, M. J.; Mayes, A. M. *Annu. Rev. Mater. Res.* **2001**, *31*, 323.
(7) Coulon, G.; Russell, T. P.; Deline, V. R.; Green, P. F. *Macromolecules* **2002**, *22*, 2581.
(8) Russell, T. P.; Coulon, G.; Deline, V. R.; Miller, D. C. *Macromolecules* **2002**, *22*, 4600.
(9) Anastasiadis, S. H.; Russell, T. P.; Satija, S. K.; Majkrzak, C. F. *Phys. Rev. Lett.* **1989**, *62*, 1852.
(10) Mansky, P.; Liu, Y.; Huang, E.; Russell, T. P.; Hawker, C. J. *Science* **1997**, *275*, 1458.

(11) Huang, E.; Rockford, L.; Russell, T. P.; Hawker, C. J. *Nature* **1998**, *395*, 757.
(12) Huang, E.; Pruzinsky, S.; Russell, T. P.; Mays, J.; Hawker, C. J. *Macromolecules* **1999**, *32*, 5299.
(13) Mansky, P.; Russell, T. P.; Hawker, C. J.; Pitsikalis, M.; Mays, J. *Macromolecules* **1997**, *30*, 6810.
(14) In, I.; La, Y. H.; Park, S. M.; Nealey, P. F.; Gopalan, P. *Langmuir* **2006**, *22*, 7855.
(15) Peters, R. D.; Yang, X. M.; Kim, T. K.; Sohn, B. H.; Nealey, P. F. *Langmuir* **2000**, *16*, 4625.
(16) Peters, R. D.; Yang, X. M.; Kim, T. K.; Nealey, P. F. *Langmuir* **2000**, *16*, 9620.
(17) Ryu, D. Y.; Shin, K.; Drockenmuller, E.; Hawker, C. J.; Russell, T. P. *Science* **2005**, *308*, 236.
(18) Han, E.; In, I.; Park, S. M.; La, Y. H.; Wang, Y.; Nealey, P. F.; Gopalan, P. *Adv. Mater.* **2007**, *19*, 4448.
(19) Bang, J.; Bae, J.; Lowenhielm, P.; Spiessberger, C.; Given-Beck, S. A.; Russell, T. P.; Hawker, C. J. *Adv. Mater.* **2007**, *19*, 4552.
(20) Son, J. G.; Bulliard, X.; Kang, H. M.; Nealey, P. F.; Char, K. *Adv. Mater.* **2008**, *20*, 3643.
(21) Jeong, S. J.; Xia, G. D.; Kim, B. H.; Shin, D. O.; Kwon, S. H.; Kang, S. W.; Kim, S. O. *Adv. Mater.* **2008**, *20*, 1898.
(22) Lee, J. K.; Char, K.; Rhee, H. W.; Ro, H. W.; Yoo, D. Y.; Yoon, D. Y. *Polymer* **2001**, *42*, 9085.
(23) Ro, H. W.; Char, K.; Jeon, E. C.; Kim, H. J.; Kwon, D.; Lee, H. J.; Lee, J. K.; Rhee, H. W.; Soles, C. L.; Yoon, D. Y. *Adv. Mater.* **2007**, *19*, 705.
(24) (a) Baney, R. H.; Itoh, M.; Sakakibara, A.; Suzuki, T. *Chem. Rev.* **1995**, *95*, 1409. (b) Brown, J. F.; Vogt, L. H.; Katchman, A.; Eustance, J. W.; Kiser, K. M.; Krantz, K. W. *J. Am. Chem. Soc.* **1960**, *82*, 6194. (c) Brown, J. F.; Prescott, P. I. *J. Am. Chem. Soc.* **2002**, *86*, 1402. (d) Frye, C. L.; Klosowski, J. M. *J. Am. Chem. Soc.* **2002**, *93*, 4599. (e) Huang, Q. R.; Volksen, W.; Huang, E.; Toney, M.; Frank, C. W.; Miller, R. D. *Chem. Mater.* **2002**, *14*, 3676.
(25) Wu, S. *J. Polym. Sci.* **1971**, *C34*, 19.
(26) (a) Busscher, H. J.; Vanpelt, A. W. J.; Deboer, P.; Dejong, H. P.; Arends, J. *Colloids Surf.* **1984**, *9*, 319.(b) van Oss, C. J. *Interfacial Forces in Aqueous Media*; CRC/Taylor & Francis: Boca Raton, FL, 2006.
(27) *Polymer Handbook*, 3rd ed.; Brandrup, J., Immergut, E. H., Eds.; John Wiley & Sons: New York, 1989.
(28) Wu, S. *Polymer Interface and Adhesion*; Marcel Dekker: New York, 1982.
(29) Busch, P.; Posselt, D.; Smilgies, D. M.; Rauscher, M.; Papadakis, C. M. *Macromolecules* **2007**, *40*, 630.
(30) Russell, T. P. *Mater. Sci. Rep.* **1990**, *5*, 171.
(31) Thurn-Albrecht, T.; Steiner, R.; DeRouchey, J.; Stafford, C. M.; Huang, E.; Bal, M.; Tuominen, M.; Hawker, C. J.; Russell, T. *Adv. Mater.* **2000**, *12*, 787.
(32) Liu, C. C.; Nealey, P. F.; Ting, Y. H.; Wendt, A. E. *J. Vac. Sci. Technol., B: Microelectron. Nanometer Struct.—Process., Meas., Phenom.* **2007**, *25*, 1963.